

Plasmon Mapping in Au@Ag Nanocube Assemblies

Bart Goris,[†] Giulio Guzzinati,[†] Cristina Fernández-López,[‡] Jorge Pérez-Juste,[‡] Luis M. Liz-Marzán,^{‡,§,||} Andreas Trügler,[#] Ulrich Hohenester,[#] Jo Verbeeck,[†] Sara Bals,^{*†} and Gustaaf Van Tendeloo[†]

[†]EMAT, University of Antwerp, Groenenborgerlaan 171, 2020 Antwerp, Belgium

[‡]Departamento de Química Física, Universidad de Vigo, 36310 Vigo, Spain

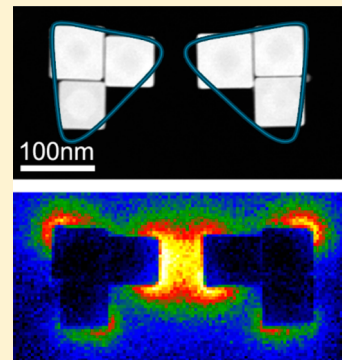
[§]BioNanoPlasmonics Laboratory, CIC biomaGUNE, Paseo de Miramón 182, 20009 Donostia - San Sebastián, Spain

^{||}Ikerbasque, Basque Foundation for Science, 48011 Bilbao, Spain

[#]Institut für Physik, Karl-Franzens-Universität Graz, Universitätsplatz 5, 8010 Graz, Austria

Supporting Information

ABSTRACT: Surface plasmon modes in metallic nanostructures largely determine their optoelectronic properties. Such plasmon modes can be manipulated by changing the morphology of the nanoparticles or by bringing plasmonic nanoparticle building blocks close to each other within organized assemblies. We report the EELS mapping of such plasmon modes in pure Ag nanocubes, Au@Ag core–shell nanocubes, and arrays of Au@Ag nanocubes. We show that these arrays enable the creation of interesting plasmonic structures starting from elementary building blocks. Special attention will be dedicated to the plasmon modes in a triangular array formed by three nanocubes. Because of hybridization, a combination of such nanotriangles is shown to provide an antenna effect, resulting in strong electrical field enhancement at the narrow gap between the nanotriangles.



1. INTRODUCTION

Plasmons are collective excitations of conduction electrons in metallic particles. For nanoparticles, the resonant surface plasmon modes are highly sensitive to the geometry of the particles and can therefore be tuned by controlling the morphology and/or the size of the structures. In this manner, nanostructures with a specific electromagnetic response can be designed, resulting in a wide variety of possible applications such as sensors¹ and nonlinear optical devices.^{2,3} Plasmon modes in metallic nanoparticles can be excited by using an optical excitation or a high-energy electron beam passing near the nanostructure. Scanning near-field optical microscopy (SNOM) can be used to visualize plasmon modes, but this technique yields limited spatial resolution (~ 50 nm) due to the aperture size of the scanning tip.⁴ When using high-energy electrons to excite the plasmon modes, spectral maps can be obtained with nanometer scale spatial resolution. Cathodoluminescence (CL) collects the emitted optical radiation and can therefore be used to map the so-called bright modes.⁵ Interestingly, a combination of bright and dark plasmon modes can be visualized when recording the energy loss of the interacting electrons.^{6,7} Due to the possibility of combining a good spatial resolution ($\sim \text{Å}$) and energy resolution (~ 0.1 eV), such electron energy loss spectroscopy (EELS) experiments performed in a scanning transmission electron microscope (STEM) recently became very popular when mapping the different surface plasmon modes in nanostructures. The technique was used to map the plasmon resonant modes in

different structures such as Au and Ag nanorods,^{8–10} Ag triangles,¹¹ Au dumbbells,¹² bow-tie antennas,¹³ nanocubes,¹⁴ and many others. As an alternative to EELS, energy filtered TEM (EFTEM) imaging, using an energy selecting slit, can be used for the mapping of plasmonic resonances as well.^{10,15} Until now, plasmon mapping was typically performed on either isolated metallic nanoparticles, dimers of nanoparticles,^{16–18} or arrays of nanoparticles synthesized by using lithography techniques.^{11,13,19,20} Electron lithography is an example of a top-down approach where a desired structure can be etched from a bulk material. However, due to the increased miniaturization of electrical and optical components, this technique becomes more challenging and time-consuming and alternatives are desirable. In this respect, the directed self-assembly of nanoparticles has been recently identified as a useful and versatile process where the building blocks become spontaneously organized into ordered structures by thermodynamic and other constraints.²¹ Directed self-assembly of nanoparticles can thus be guided by either tailoring the intrinsic features of nanoparticles,²² an external force that induces and guides the self-assembly,²³ or a combination of both.²⁴ Recently, plasmon mapping has been applied to linear chains of nanoparticles^{25,26} and on clusters of nanoparticles assembled on DNA strands,²⁷ but these results have only been

Received: March 14, 2014

Revised: June 27, 2014

Published: June 27, 2014



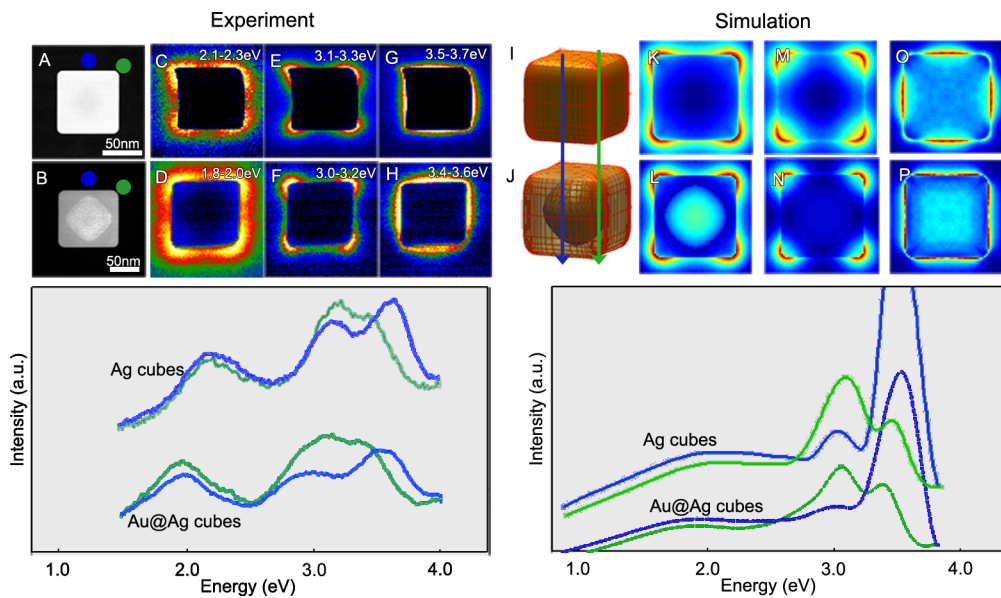


Figure 1. Comparison of plasmon modes between Au@Ag and Ag nanocubes. Both experimental data (left) and BEM simulations (right) indicate that there are only small differences between the response of Au@Ag core–shell nanocubes and pure Ag nanocubes. Both particles show three distinct plasmon modes that are most easily excited at either the corners or the edges of the nanocubes. The energy loss of the different modes can be observed in the background subtracted experimental and simulated energy loss spectra. These spectra are acquired at the positions that are indicated in panels A, B, I, and J. The color map is scaled between 0 and the maximum value which equals 0.171%, 0.447%, 0.496%, 0.145%, 0.263%, and 0.290% of the total integrated intensity for panels C–H, respectively.

obtained on spherical nanoparticles yielding a limited number of plasmon resonances.

In this work, we carried out a detailed characterization of ordered Au@Ag nanocube arrays by high-angle annular dark field (HAADF) STEM imaging and EELS, which revealed interesting plasmonic properties with an increased flexibility as compared to their single particle counterparts. This is of great importance since self-assembly may lead to well-defined assemblies with a variety of morphologies, thereby offering the possibility to observe unusual modes by plasmon coupling. Au@Ag core–shell structures are of high interest because of the increased field enhancement provided by Ag nanoparticles as compared to, for example, Au or Cu.^{28,29} In the particular case of Au octahedrons, it has been reported that silver growth leads to an external cubic morphology.²⁸ Ag nanocubes and their assemblies can be used for various plasmonic applications, for example, as substrates for surface-enhanced Raman scattering (SERS)^{30–33} or as plasmonic reporters of molecular chirality.³⁴

2. EXPERIMENTAL SECTION

The individual nanocubes were synthesized by the seeded growth of Ag on preformed Au nanoparticles with octahedral shape.³⁵ More details about the sample preparation can be found in the Supporting Information. The average size of the Au@Ag nanocubes is approximately 70 nm whereas the length of a [110] ribbon in the octahedron equals 36 nm.

For the mapping of the plasmon resonances, HAADF-STEM imaging is combined with monochromated STEM-EELS. Using HAADF-STEM, a fine electron probe scans across the sample. All the electrons that have scattered to relatively large angles are collected, yielding an image in which the intensity scales with the thickness of the sample and with a power of the average atomic number of the atoms in the sample $Z^{1.7}$.^{36–38} In STEM-EELS the probe is scanned while the transmitted beam is collected in a spectrometer, recording an electron energy loss

spectrum for every pixel in the raster which allows the point by point measurement of the energy loss probability to be measured. All experiments were performed on an aberration-corrected cubed FEI Titan 50–80. The microscope was operated at a high tension of 300 kV, using a probe semiconvergence angle of 21.4 mrad. During the acquisition, a monochromated electron probe is used yielding a fwhm of the zero-loss peak of 0.17 eV. For the acquisition of the plasmon maps, a pixel size of 2 nm is used with a spectrum collection time of 0.02 s. To extract quantitative information from the spectra, they are normalized by dividing each spectrum by its integrated intensity. Next, a power law background model is applied to estimate the contribution of the zero-loss peak. Plasmon maps are obtained by using an energy selecting window that is positioned at the desired energy losses (width = 0.2 eV).

The theoretical simulations of the plasmon modes are performed with the MNPBEM toolbox based on the boundary element method (BEM).^{39–42} Within this simulation method the boundaries between different materials are discretized by using a geometrical mesh, and then the Maxwell equations are solved by using these boundary conditions. The MNPBEM toolbox adopts in particular a potential based approach that employs the Maxwell equations for the scalar and vector potential, thus reducing the number of components that need to be considered. The dielectric functions of Au and Ag are extracted from optical data.⁴³ The influence of the SiN support is neglected in the simulations.

3. RESULTS AND DISCUSSION

3.1. Plasmon Mapping on Isolated Cubes. The use of Au@Ag nanocubes in comparison to pure Ag nanocubes provides access to a larger size range, which facilitates the formation of arrays on the TEM grids.⁴⁴ However, the presence of the Au octahedron core may also influence the plasmon

modes of single nanocubes. For comparison, pure Ag nanocubes of similar (slightly smaller) dimensions were synthesized by the polyol method. A HAADF STEM projection of both types of particles is displayed in Figure 1, with the heavier Au core appearing brighter than the Ag shell in Figure 1B. For both structures, EEL spectra were recorded at different locations, revealing the presence of multiple plasmon resonances, as previously reported.¹⁴ The background subtracted spectra are displayed in Figure 1, whereas the unprocessed spectra are displayed in the Supporting Information (Figure S1). The background subtracted spectra show three distinct plasmon resonances at energy values of 2.2, 3.2, and 3.6 eV (corresponding to wavelengths equal to 564, 387, and 354 nm, respectively) for the pure Ag nanocubes and at 1.9, 3.1, and 3.5 eV (653, 400, and 354 nm) for the Au@Ag core–shell nanocubes. Note that the peak at 3.1 eV seems to shift depending on the spatial position of the electron probe resulting in a shoulder in the spectra. However, this shift is only apparent and caused by the tails of the neighboring peaks as demonstrated with a fit to three Lorentzians at fixed energies in Figure S2, Supporting Information.

The UV–vis spectra from solutions containing the Au@Ag nanocubes are displayed in the Supporting Information, Figure S3. Using these energy values, a map of each plasmon mode was obtained as reported in the Experimental Section. It can be seen that the two modes with the lowest energy have the highest probability to be excited at the corners of the particles, whereas the third mode is best excited at the side faces. This probability is related to the modulus squared of the component of the local field enhancement parallel to the beam direction.⁴⁵

Further insight into these observations was obtained by comparing the experimental data to simulations. It must be noted that the energy resolution of these simulations is better because they do not suffer from experimental limitations. As can be seen from Figure 1, both the calculated energy levels and the spatial distribution of the energy loss probability are in good agreement with the experiments. After comparison of the experimental spectra of Au@Ag core–shell nanocubes with those of pure Ag nanocubes, it can be concluded that the influence of the Au core is negligible for this type of nanostructures within the present dimensions and thus pure silver nanocubes were considered for the BEM simulations in the remainder of this work.

3.2. Plasmon Mapping on Arrays of Nanocubes. When the Au@Ag nanocube dispersion was dried on a 30 nm thick SiN support grid, particles were found to self-assemble into a variety of ordered structures where a side-by-side arrangement is most commonly observed. A few examples of such assemblies yielding remarkable plasmonic properties are presented in the Supporting Information, Figure S4. As a first example, localized plasmon modes were investigated for a dimer of nanocubes located side-by-side, with a separation of 4–5 nm (Figure 2). This system has been previously discussed, both theoretically^{44,46} and experimentally by near-field optical imaging techniques.⁴⁷ The acquired EEL spectra of the nanocubes dimer is displayed in Figure 2 and reveals six major plasmon modes. The lowest energy mode corresponds to the dipolar mode of a (square) nanorod with a length that equals the sum of the length of the nanocubes, in agreement with previous studies.^{46,48} The other five modes are more localized on either the corners or the sides of the nanocubes. The spatial distributions of all these modes are again in qualitative agreement with BEM simulations, as presented in Figure 2.

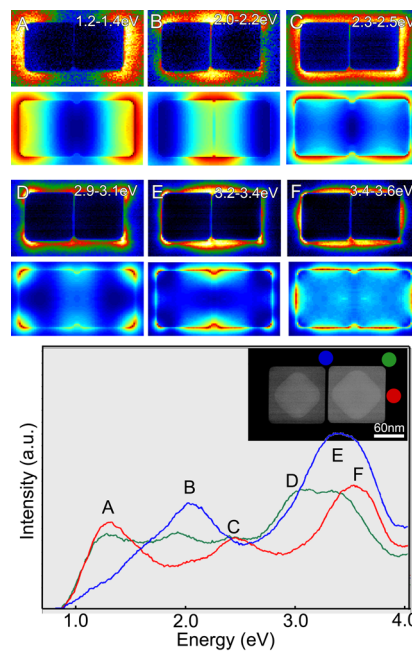


Figure 2. Plasmon mapping of a dimer made of two Au@Ag core–shell nanocubes. The HAADF-STEM projection in the inset shows that the nanocubes tend to orient themselves side by side even when they are not in direct contact. The low loss EEL spectra were acquired at the positions indicated in the inset, with the same color as the actual spectra. From these spectra, six major plasmon modes are identified and labeled from A to F. The experimental plasmon maps are in good qualitative agreement with the BEM simulations. The color map is scaled between 0 and the maximum value of the percentage of the summed spectra which equals 0.149%, 0.176%, 0.178%, 0.247%, 0.286%, and 0.294% for panels A–F, respectively.

Due to the side-by-side arrangement of the individual nanocubes, a variety of large regular arrays can be found. An example is an array of 6 nanocubes that are organized in a 2×3 matrix, which is displayed in Figure 3. In addition, linear chains of nanocubes are presented in this figure as well with a length of 2 and 3 nanocubes. It is interesting to compare maps obtained at the same energy losses from these three structures. The acquired spectra are presented in Figure S5, Supporting Information. As can be observed, the modes of the array along the two orthogonal directions display the same symmetry as the modes of the isolated linear chains. This is due to the fact that the arrayed structure is quantized in two orthogonal directions where the quantization condition along the two axes corresponds to those of arrays of 3×1 and 2×1 nanocubes, respectively.

To understand this phenomenon, BEM simulations, as presented in the Supporting Information (Figure S6), have been performed indicating that the plasmon modes of an array of 2×3 nanocubes are similar to those of a single rectangular particle with the same outer dimensions as the array. When the gap size between the particles is small in comparison to the wavelength of the plasmon mode, the influence of the gap on the mode is negligible and the response of the total structure can be understood qualitatively as if the gaps were not present. Deviations from this qualitative model are expected to be significant only at plasmon modes which are located at higher energy losses. These findings open up the opportunities to construct large nanostructures based on single nanocubes and

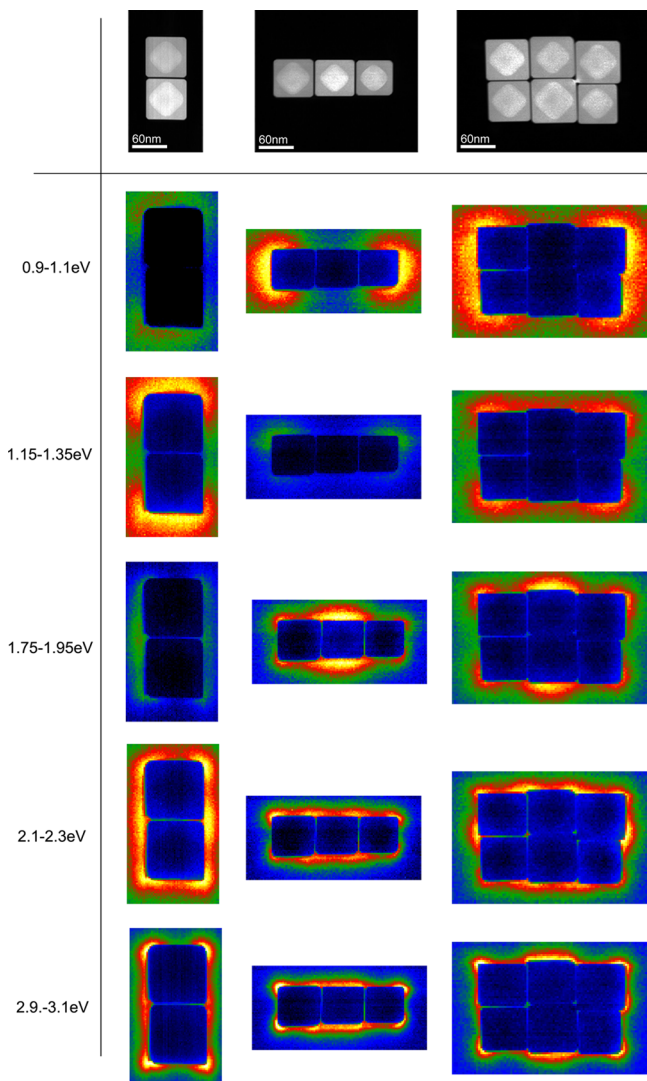


Figure 3. Plasmon modes of both linear and 2D arrays of nanocubes. Since the quantization condition of such a rectangular array is a combination of the quantization conditions in the isolated chains, the frequencies at which the different plasmon resonances occur are related as well. The color code is kept constant in each row to enable a comparison of the intensities between the three different plasmonic structures.

conversely to describe the plasmonic behavior of a large superstructure as that of a single larger structure.

The previous examples show that the plasmonic properties of the assemblies are similar to those of a larger continuous system with the same shape and size as the structure formed by the individual nanocubes, enabling the synthesis of structures with tailored plasmonic properties in a more flexible manner by starting from elementary building blocks.

Interestingly, 3 nanocubes may form an approximately triangular array, as shown in Figure 4, in which the acquired EEL spectra at three different positions are also displayed. The plasmon maps that are extracted from the measurements are again in good agreement with those simulated for the same morphology. From these maps (Figure 4a,b), it can be observed that the main plasmon modes are obtained at energy losses of 1.2 and 1.6 eV and are in qualitative agreement to the plasmon modes of a nanotriangle.¹¹ At higher energy losses, the plasmon modes have a shorter wavelength, and are therefore more

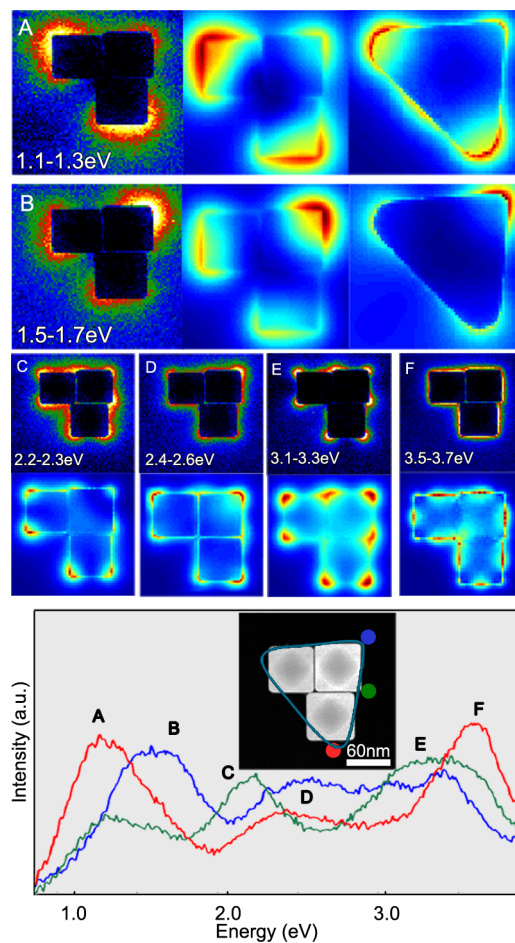


Figure 4. Surface plasmon modes of a triangle comprising three Au@Ag core–shell nanocubes. The inset shows a HAADF-STEM projection from three Au@Ag core–shell nanocubes that are arranged in a triangular shape. Panels A and B show the correspondence between the plasmon modes of the experimental investigated structure and an ideal nanotriangle. The unprocessed EELS spectra were acquired at the positions indicated by the dots of the corresponding colors. When inspecting these spectra, several modes are observed, which are in qualitative agreement with BEM simulations (A–F). The color map is scaled between 0 and the maximum value of the percentage of the summed spectra which equals 0.107%, 0.131%, 0.156%, 0.169%, 0.245%, and 0.313% for panels A–F, respectively.

strongly influenced by deviations from a perfect triangular structure.⁴⁹ This results in multiple regions of high intensity that are mainly located at the corners of the individual cubes as can also be appreciated from the experimental maps and simulations included in Figure 4, clearly demonstrating the difference between a perfect triangle and the structure that was investigated experimentally. It is obvious that a more accurate triangular shape can be obtained when using more nanocubes. A triangle resulting from the self-assembly of 6 individual nanocubes instead of 3 was found in this sample as well and the plasmon mapping is displayed in the Supporting Information, Figure S7.

A nanotriangle constructed as illustrated in Figure 4 could possibly act as the first half of a simplified bow-tie antenna. The bow-tie antenna structure consists of two triangular parts where the corner of the first triangle points toward a corner of the second triangle. In the present case, the gap between both triangular structures equals 56 nm. Such an antenna has great

potential due to the field enhancement in the central region between the two triangles caused by plasmon coupling.^{13,50} Field enhancement has found important applications for example in single molecule sensors or for the fabrication of optical antennas.^{50,51} The ordering of the nanocubes occasionally leads to the formation of such an antenna as illustrated in Figure 5. Even with the simplified geometry, where each

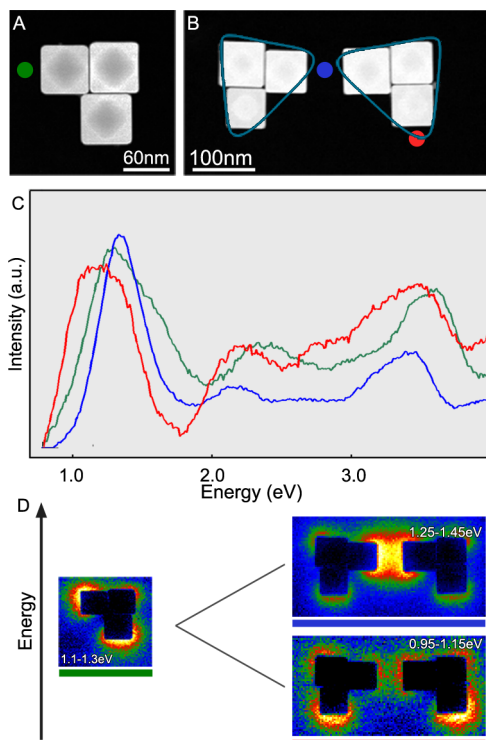


Figure 5. Hybridization of plasmon modes at a bow-tie antenna structure obtained by a specific order of self-assembled nanocubes. When two triangular structures (A) are approaching (B), hybridization splits the original lowest energy plasmon mode into two separate modes; a symmetric and an antisymmetric mode with an energy that is shifted downward or upward, respectively.

triangle comprises 3 cubes only, the field enhancement due to the coupling can be clearly visualized in the center of both the experimental and the simulated plasmon maps. As presented in Figure 5, the field enhancement is caused by hybridization of the plasmon mode (at 1.2 eV) of the individual structures yielding a symmetric state at 1.1 eV and an antisymmetric state at 1.35 eV, respectively. For these states, the loss probability is respectively reduced and strongly increased in the region between the two triangular structures when compared to the isolated triangle. This is in agreement with previous studies where hybridization between different nanostructures was characterized.^{52,53} As reported in the literature, the difference in energy between the two hybridization modes increases with a decreasing width between the two structures, meaning that the energy at which the field enhancement is maximal shifts as a monotonic function of the gap width.⁵² This is confirmed by simulations as presented in Figure S8, Supporting Information. In addition, the BEM simulations of the field enhancement in Figure S8 (Supporting Information) provide useful information to optimize the design of such an antenna constructed from individual nanocubes. For different gap sizes between the two structures, the energy loss probability is simulated in the region

between the two triangular structures. The results indicate that the energy loss probability of the incoming electrons reaches a maximum when the gap between the two structures equals 35 nm. A larger or a smaller gap results in a decrease of the signal. When the energy loss measurements are compared to the field enhancement obtained by an optical excitation, some differences are observed, since for optical excitations the maximum in the field enhancement tends to increase with a decreasing gap length between neighboring structures.^{51,54,55} The differences between optical excitations and excitations caused by fast electron beams have been discussed theoretically by Hohenester and co-workers.⁵⁶

The plasmon modes present in the spectrum acquired at higher energy losses (>2 eV) are more localized and therefore less influenced by the coupling of both structures. As a consequence, their spatial extent remains comparable to the modes of a single triangle. These plasmon modes are displayed in the Supporting Information, Figure S9.

In this paper, the arrays of nanostructures were obtained by self-assembly of the nanocubes on a SiN support grid resulting in a side-by-side arrangement. Previously, it has been shown by several groups that control over this ordering process can be achieved by modification of the polymers (or other capping ligands) that are attached to the side facets of the individual particles,⁴⁴ e.g., by using specific DNA sequences^{57,58} or by using template matching assembly on a predefined substrate.^{30,59} For example, Xia and co-workers recently reported the creation of specific predefined structures from Ag nanocubes by modifying their side facets with hydrophobic and/or hydrophilic monolayers.⁶⁰ As presented in this work, this opens up the possibility to obtain assemblies that yield useful plasmonic applications.⁶¹

4. CONCLUSION

In conclusion, we have shown that arrays of Au@Ag core–shell nanocubes constitute a valid alternative to lithography methods for the fabrication of relatively complex structures with interesting plasmonic properties, based on the self-assembly of elementary building blocks. As an example, we investigated regular arrays of Ag nanocubes, as well as compositions of triangles made of several nanocubes. We demonstrated that two of these triangles can be used to obtain a bow-tie antenna that leads to a large field enhancement in the spatial region between both triangles.

■ ASSOCIATED CONTENT

■ Supporting Information

Details on sample preparation, a comparison between EELS data before and after background subtraction, EELS data fitted to a model of three Lorentzian curves, UV-vis spectra, an overview of different geometries obtained from nanocubes, the energy loss spectra for the 2×3 array, a comparison between a 2×3 array and a single particle, a STEM image of a triangular shape obtained from 6 nanocubes, an image showing the energy shift in the bow-tie antenna, and plasmon maps of the higher order modes of the bow-tie antenna. This material is available free of charge via the Internet at <http://pubs.acs.org>.

■ AUTHOR INFORMATION

Corresponding Author

*E-mail: sara.bals@uantwerpen.be.

Notes

The authors declare no competing financial interest.

ACKNOWLEDGMENTS

The work was supported by the Flemish Fund for Scientific Research (FWO Vlaanderen) through a Ph.D. research grant to B.G. The authors acknowledge financial support from the European Research Council (ERC Advanced Grant 24691-COUNTATOMS, ERC Advanced Grant 267867-PLASMA-QUO, ERC Starting Grant 278510-VORTEX, and ERC Starting Grant 335078-COLOURATOMS). The authors also appreciate financial support from the European Union under the Seventh Framework Program (Integrated Infrastructure Initiative N. 262348 European Soft Matter Infrastructure, ESMI). This work has been supported by the Austrian Science Fund FWF under project P24511 and the SFB NextLite. The authors acknowledge Prof. Dr. F. J. G. de Abajo for fruitful discussions.

REFERENCES

- (1) Sherry, L. J.; Chang, S. H.; Schatz, G. C.; Van Duyne, R. P.; Wiley, B. J.; Xia, Y. N. Localized Surface Plasmon Resonance Spectroscopy of Single Silver Nanocubes. *Nano Lett.* **2005**, *5*, 2034–2038.
- (2) Pendry, J. B.; Holden, A. J.; Robbins, D. J.; Stewart, W. J. Magnetism from Conductors and Enhanced Nonlinear Phenomena. *IEEE Trans. Microwave Theory Tech.* **1999**, *47*, 2075–2084.
- (3) Klein, M. W.; Enkrich, C.; Wegener, M.; Linden, S. Second-Harmonic Generation from Magnetic Metamaterials. *Science* **2006**, *313*, 502–504.
- (4) Lewis, A.; Taha, H.; Strikovski, A.; Manevitch, A.; Khatchatourians, A.; Dekhter, R.; Ammann, E. Near-Field Optics: From Subwavelength Illumination to Nanometric Shadowing. *Nat. Biotechnol.* **2003**, *21*, 1377–1386.
- (5) Kuttge, M.; Vesseur, E. J. R.; Polman, A. Fabry-Perot Resonators for Surface Plasmon Polaritons Probed by Cathodoluminescence. *Appl. Phys. Lett.* **2009**, *94*, 183104.
- (6) Myroshnychenko, V.; Nelayah, J.; Adamo, G.; Geuquet, N.; Rodriguez-Fernandez, J.; Pastoriza-Santos, I.; MacDonald, K. F.; Henrard, L.; Liz-Marzan, L. M.; Zheludev, N. I.; et al. Plasmon Spectroscopy and Imaging of Individual Gold Nanodecahedra: A Combined Optical Microscopy, Cathodoluminescence, and Electron Energy-Loss Spectroscopy Study. *Nano Lett.* **2012**, *12*, 4172–4180.
- (7) de Abajo, F. J. G. Optical Excitations in Electron Microscopy. *Rev. Mod. Phys.* **2010**, *82*, 209–275.
- (8) Schaffer, B.; Hohenester, U.; Trugler, A.; Hofer, F. High-Resolution Surface Plasmon Imaging of Gold Nanoparticles by Energy-Filtered Transmission Electron Microscopy. *Phys. Rev. B* **2009**, *79*, 041401.
- (9) Nicoletti, O.; Wubs, M.; Mortensen, N. A.; Sigle, W.; van Aken, P. A.; Midgley, P. A. Surface Plasmon Modes of a Single Silver Nanorod: An Electron Energy Loss Study. *Opt. Express* **2011**, *19*, 15371–15379.
- (10) N'gom, M.; Li, S. Z.; Schatz, G.; Erni, R.; Agarwal, A.; Kotov, N.; Norris, T. B. Electron-Beam Mapping of Plasmon Resonances in Electromagnetically Interacting Gold Nanorods. *Phys. Rev. B* **2009**, *80*, 113411.
- (11) Nelayah, J.; Kociak, M.; Stephan, O.; de Abajo, F. J. G.; Tence, M.; Henrard, L.; Taverna, D.; Pastoriza-Santos, I.; Liz-Marzan, L. M.; Colliex, C. Mapping Surface Plasmons on a Single Metallic Nanoparticle. *Nat. Phys.* **2007**, *3*, 348–353.
- (12) Rodriguez-Gonzalez, B.; Attouchi, F.; Cardinal, M. F.; Myroshnychenko, V.; Stephan, O.; de Abajo, F. J. G.; Liz-Marzan, L. M.; Kociak, M. Surface Plasmon Mapping of Dumbbell-Shaped Gold Nanorods: The Effect of Silver Coating. *Langmuir* **2012**, *28*, 9063–9070.
- (13) Koh, A. L.; Fernandez-Dominguez, A. I.; McComb, D. W.; Maier, S. A.; Yang, J. K. W. High-Resolution Mapping of Electron-Beam-Excited Plasmon Modes in Lithographically Defined Gold Nanostructures. *Nano Lett.* **2011**, *11*, 1323–1330.
- (14) Mazzucco, S.; Geuquet, N.; Ye, J.; Stephan, O.; Van Roy, W.; Van Dorpe, P.; Henrard, L.; Kociak, M. Ultralocal Modification of Surface Plasmons Properties in Silver Nanocubes. *Nano Lett.* **2012**, *12*, 1288–1294.
- (15) Schaffer, B.; Grogger, W.; Kothleitner, G.; Hofer, F. Comparison of ETEM and STEM EELS Plasmon Imaging of Gold Nanoparticles in a Monochromated TEM. *Ultramicroscopy* **2010**, *110*, 1087–1093.
- (16) Bigelow, N. W.; Vaschillo, A.; Iberi, V.; Camden, J. P.; Masiello, D. J. Characterization of the Electron- and Photon-Driven Plasmonic Excitations of Metal Nanorods. *ACS Nano* **2012**, *6*, 7497–7504.
- (17) Koh, A. L.; Bao, K.; Khan, I.; Smith, W. E.; Kothleitner, G.; Nordlander, P.; Maier, S. A.; McComb, D. W. Electron Energy-Loss Spectroscopy (EELS) of Surface Plasmons in Single Silver Nanoparticles and Dimers: Influence of Beam Damage and Mapping of Dark Modes. *ACS Nano* **2009**, *3*, 3015–3022.
- (18) Scholl, J. A.; Garcia-Etxarri, A.; Koh, A. L.; Dionne, J. A. Observation of Quantum Tunneling Between Two Plasmonic Nanoparticles. *Nano Lett.* **2013**, *13*, 564–569.
- (19) Wiener, A.; Duan, H.; Bosman, M.; Horsfield, A. P.; Pendry, J. B.; Yang, J. K.; Maier, S. A.; Fernandez-Dominguez, A. I. Electron-Energy Loss Study of Nonlocal Effects in Connected Plasmonic Nanoprisms. *ACS Nano* **2013**, *7*, 6287–6296.
- (20) Koller, D. M.; Hohenester, U.; Hohenau, A.; Ditlbacher, H.; Reil, F.; Galler, N.; Aussenegg, F. R.; Leitner, A.; Trugler, A.; Krenn, J. R. Superresolution Moire Mapping of Particle Plasmon Modes. *Phys. Rev. Lett.* **2010**, *104*, 143901.
- (21) Grzelczak, M.; Vermant, J.; Furst, E. M.; Liz-Marzan, L. M. Directed Self-Assembly of Nanoparticles. *ACS Nano* **2010**, *4*, 3591–3605.
- (22) Guerrero-Martinez, A.; Perez-Juste, J.; Carbo-Argibay, E.; Tardajos, G.; Liz-Marzan, L. M. Gemini-Surfactant-Directed Self-Assembly of Monodisperse Gold Nanorods into Standing Superlattices. *Angew. Chem., Int. Ed.* **2009**, *48*, 9484–9488.
- (23) Ding, T.; Song, K.; Clays, K.; Tung, C. H. Fabrication of 3d Photonic Crystals of Ellipsoids: Convective Self-Assembly in Magnetic Field. *Adv. Mater.* **2009**, *21*, 1936–1940.
- (24) Sanchez-Iglesias, A.; Grzelczak, M.; Altantzis, T.; Goris, B.; Perez-Juste, J.; Bals, S.; Van Tendeloo, G.; Donaldson, S. H.; Chmelka, B. F.; Israelachvili, J. N.; et al. Hydrophobic Interactions Modulate Self-Assembly of Nanoparticles. *ACS Nano* **2012**, *6*, 11059–11065.
- (25) Qin, Y.; Vogelgesang, R.; Esslinger, M.; Sigle, W.; van Aken, P.; Moutanabbir, O.; Knez, M. Bottom-up Tailoring of Plasmonic Nanopeapods Making Use of the Periodical Topography of Carbon Nanocoil Templates. *Adv. Funct. Mater.* **2012**, *22*, 5157–5165.
- (26) Barrow, S. J.; Rossouw, D.; Funston, A. M.; Botton, G. A.; Mulvaney, P. Mapping Bright and Dark Modes in Gold Nanoparticle Chains Using Electron Energy Loss Spectroscopy. *Nano Lett.* [Online early access]. DOI: 10.1021/ja047915o. Published Online: June 23, 2014. <http://pubs.acs.org/doi/abs/10.1021/ja047915o> (accessed June 24, 2014).
- (27) Diaz-Egea, C.; Sigle, W.; van Aken, P.; Molina, S. High Spatial Resolution Mapping of Surface Plasmon Resonance Modes in Single and Aggregated Gold Nanoparticles Assembled on DNA Strands. *Nanoscale Res. Lett.* **2013**, *8*, 337.
- (28) Jiang, R. B.; Chen, H. J.; Shao, L.; Li, Q.; Wang, J. F. Unraveling the Evolution and Nature of the Plasmons in (Au Core)-(Ag Shell) Nanorods. *Adv. Mater.* **2012**, *24*, 200–207.
- (29) Rycenga, M.; Cobley, C. M.; Zeng, J.; Li, W. Y.; Moran, C. H.; Zhang, Q.; Qin, D.; Xia, Y. N. Controlling the Synthesis and Assembly of Silver Nanostructures for Plasmonic Applications. *Chem. Rev.* **2011**, *111*, 3669–3712.
- (30) Fang, C.; Brodoceanu, D.; Kraus, T.; Voelcker, N. H. Templated Silver Nanocube Arrays for Single-Molecule SERS Detection. *RSC Adv.* **2013**, *3*, 4288–4293.

- (31) Fu, Q.; Zhang, D. G.; Chen, Y. K.; Wang, X. X.; Han, L.; Zhu, L. F.; Wang, P.; Ming, H. Surface Enhanced Raman Scattering Arising from Plasmonic Interaction Between Silver Nano-Cubes and a Silver Grating. *Appl. Phys. Lett.* **2013**, *103*, 041122.
- (32) Lee, S. Y.; Hung, L.; Lang, G. S.; Cornett, J. E.; Mayergoyz, I. D.; Rabin, O. Dispersion in the Sers Enhancement with Silver Nanocube Dimers. *ACS Nano* **2010**, *4*, 5763–5772.
- (33) Rycenga, M.; Xia, X. H.; Moran, C. H.; Zhou, F.; Qin, D.; Li, Z. Y.; Xia, Y. A. Generation of Hot Spots with Silver Nanocubes for Single-Molecule Detection by Surface-Enhanced Raman Scattering. *Angew. Chem., Int. Ed.* **2011**, *50*, 5473–5477.
- (34) Lu, F.; Tian, Y.; Liu, M.; Su, D.; Zhang, H.; Govorov, A. O.; Gang, O. Discrete Nanocubes as Plasmonic Reporters of Molecular Chirality. *Nano Lett.* **2013**, *13*, 3145–3151.
- (35) Gómez-Graña, S.; Goris, B.; Altantzis, T.; Fernández-López, C.; Carbó-Argibay, E.; Guerrero-Martínez, A.; Almora-Barrios, N.; Carbó-Argibay, E.; Guerrero-Martínez, A.; Almora-Barrios, N.; et al. Au@Ag Nanoparticles: Halides Stabilize {100} Facets. *J. Phys. Chem. Lett.* **2013**, *4*, 2209–2216.
- (36) Hartel, P.; Rose, H.; Dinges, C. Conditions and Reasons for Incoherent Imaging in STEM. *Ultramicroscopy* **1996**, *63*, 93–114.
- (37) Krivanek, O. L.; Chisholm, M. F.; Nicolosi, V.; Pennycook, T. J.; Corbin, G. J.; Dellby, N.; Murfitt, M. F.; Own, C. S.; Szilagyi, Z. S.; Oxley, M. P.; et al. Atom-by-Atom Structural and Chemical Analysis by Annular Dark-Field Electron Microscopy. *Nature* **2010**, *464*, 571–574.
- (38) Nellist, P. D.; Pennycook, S. J. The Principles and Interpretation of Annular Dark-Field Z-Contrast Imaging. *Adv. Imaging Electron Phys.* **2000**, *113*, 147–203.
- (39) de Abajo, F. J. G.; Howie, A. Retarded Field Calculation of Electron Energy Loss in Inhomogeneous Dielectrics. *Phys. Rev. B* **2002**, *65*, 115418.
- (40) Hohenester, U.; Krenn, J. R. Surface Plasmon Resonances of Single and Coupled Metallic Nanoparticles: A Boundary Integral Method Approach. *Phys. Rev. B* **2005**, *72*, 195429.
- (41) Hohenester, U.; Trugler, A. Mnpbem - a Matlab Toolbox for the Simulation of Plasmonic Nanoparticles. *Comput. Phys. Commun.* **2012**, *183*, 370–381.
- (42) Hohenester, U. Simulating Electron Energy Loss Spectroscopy with the Mnpbem Toolbox. *Comput. Phys. Commun.* **2014**, *185*, 1177–1187.
- (43) Palik, E. D. *Handbook of Optical Constants of Solids II*; Academic Press: Boston, MA, 1991; p 1096.
- (44) Gao, B.; Arya, G.; Tao, A. R. Self-Orienting Nanocubes for the Assembly of Plasmonic Nanojunctions. *Nat. Nanotechnol.* **2012**, *7*, 433–437.
- (45) Boudarham, G.; Kociak, M. Modal Decompositions of the Local Electromagnetic Density of States and Spatially Resolved Electron Energy Loss Probability in Terms of Geometric Modes. *Phys. Rev. B* **2012**, *85*, 245447.
- (46) Grillet, N.; Manchon, D.; Bertorelle, F.; Bonnet, C.; Broyer, M.; Cottancin, E.; Lerme, J.; Hillenkamp, M.; Pellarin, M. Plasmon Coupling in Silver Nanocube Dimers: Resonance Splitting Induced by Edge Rounding. *ACS Nano* **2011**, *5*, 9450–9462.
- (47) Kim, D. S.; Heo, J.; Ahn, S. H.; Han, S. W.; Yun, W. S.; Kim, Z. H. Real-Space Mapping of the Strongly Coupled Plasmons of Nanoparticle Dimers. *Nano Lett.* **2009**, *9*, 3619–3625.
- (48) Cortie, M. B.; Liu, F. G.; Arnold, M. D.; Niidome, Y. Multimode Resonances in Silver Nanocuboids. *Langmuir* **2012**, *28*, 9103–9112.
- (49) Schmidt, F. P.; Ditzbacher, H.; Hohenester, U.; Hohenau, A.; Hofer, F.; Krenn, J. R. Universal Dispersion of Surface Plasmons in Flat Nanostructures. *Nat. Commun.* **2014**, *5*, 3604.
- (50) Esteban, R.; Borisov, A. G.; Nordlander, P.; Aizpurua, J. Bridging Quantum and Classical Plasmonics with a Quantum-Corrected Model. *Nat. Commun.* **2012**, *3*, 825.
- (51) Yu-Ming, W.; Le-Wei, L.; Bo, L., Geometric Effects in Designing Bow-Tie Nanoantenna for Optical Resonance Investigation. In *2010 Asia Pacific International Symposium on Electromagnetic Compatibility*, Beijing, China, 2010.
- (52) Nordlander, P.; Oubre, C.; Prodan, E.; Li, K.; Stockman, M. I. Plasmon Hybridization in Nanoparticle Dimers. *Nano Lett.* **2004**, *4*, 899–903.
- (53) von Cube, F.; Irsen, S.; Diehl, R.; Niegemann, J.; Busch, K.; Linden, S. From Isolated Metaatoms to Photonic Metamaterials: Evolution of the Plasmonic near-Field. *Nano Lett.* **2013**, *13*, 703–708.
- (54) Fromm, D. P.; Sundaramurthy, A.; Schuck, P. J.; Kino, G.; Moerner, W. E. Gap-Dependent Optical Coupling of Single "Bowtie" Nanoantennas Resonant in the Visible. *Nano Lett.* **2004**, *4*, 957–961.
- (55) Hatab, N. A.; Hsueh, C. H.; Gaddis, A. L.; Retterer, S. T.; Li, J. H.; Eres, G.; Zhang, Z. Y.; Gu, B. H. Free-Standing Optical Gold Bowtie Nanoantenna with Variable Gap Size for Enhanced Raman Spectroscopy. *Nano Lett.* **2010**, *10*, 4952–4955.
- (56) Hohenester, U.; Ditzbacher, H.; Krenn, J. R. Electron-Energy-Loss Spectra of Plasmonic Nanoparticles. *Phys. Rev. Lett.* **2009**, *103*, 106801.
- (57) Ke, Y. G.; Ong, L. L.; Shih, W. M.; Yin, P. Three-Dimensional Structures Self-Assembled from DNA Bricks. *Science* **2012**, *338*, 1177–1183.
- (58) Macfarlane, R. J.; Lee, B.; Jones, M. R.; Harris, N.; Schatz, G. C.; Mirkin, C. A. Nanoparticle Superlattice Engineering with DNA. *Science* **2011**, *334*, 204–208.
- (59) Fan, J. A.; Wu, C. H.; Bao, K.; Bao, J. M.; Bardhan, R.; Halas, N. J.; Manoharan, V. N.; Nordlander, P.; Shvets, G.; Capasso, F. Self-Assembled Plasmonic Nanoparticle Clusters. *Science* **2010**, *328*, 1135–1138.
- (60) Rycenga, M.; McLellan, J. M.; Xia, Y. N. Controlling the Assembly of Silver Nanocubes Through Selective Functionalization of Their Faces. *Adv. Mater.* **2008**, *20*, 2416–2420.
- (61) Jageler-Hoheisel, T.; Cordeiro, J.; Lecarme, O.; Cuche, A.; Girard, C.; Dujardin, E.; Peyrade, D.; Arbouet, A. Plasmonic Shaping in Gold Nanoparticle Three-Dimensional Assemblies. *J. Phys. Chem. C* **2013**, *117*, 23126–23132.